

MODIS-based Change Detection for Grizzly Bear Habitat Mapping in Alberta

Alysha D. Pape and Steven E. Franklin

Abstract

Coarse resolution data from the Moderate Resolution Imaging Spectroradiometer (MODIS) was used to test the effectiveness of 250 m data to detect forest disturbances and update an existing, large-area (150,000 km²), 30 m Landsat ETM+ and TM land-cover map product used in Grizzly Bear (*Ursus arctos*) habitat analysis. A Landsat-derived polygon layer was applied to the MOD13Q1 data product to create a polygon-based, mean NDVI time series (2000 to 2005). Image differencing of the dataset produced multiple-scale layers of change including a two-date, five-year change and a five-year composite of annual changes. Accuracy assessments based on available GIS data showed an overall accuracy as high as 59 percent. Results also show that disturbance patches larger than 15 ha were represented with an accuracy of 75 percent or higher. This offers an alternative to higher spatial resolution data for the identification of larger features and also provides general change information for those areas that may be suitable for analysis with higher spatial resolution data.

Introduction

Forests are subject to change from anthropogenic activities such as mining, forestry, recreation, and oil and gas exploration. The impacts of these activities often cover large areas and may have a negative influence on the natural processes of ecosystems and habitats that exist in these areas (Lunetta, 1998; Yuan *et al.*, 1998; Gong and Xu, 2003; Wulder *et al.*, 2003; Wessels *et al.*, 2004; Fraser *et al.*, 2005; Jensen, 2005; Linke, 2006). With these activities expanding deeper into environmentally sensitive areas, public interest in the health and status of these ecosystems can also generate pressure for more accurate monitoring and sustainable management practices. An example is the Foothills Model Forest (FMF) Grizzly Bear Research Project (GBRP). One goal of the GBRP is to map the entire grizzly bear range in Alberta Figure 1 using 30 m Landsat TM and ETM+ imagery in an effort to determine the relationship between grizzly bear response and health to intensive land-use activities (Stenhouse and Graham, 2005). Originally, a core study area of roughly 10,000 square kilometers in 1999, it has since expanded to over 250,000 square kilometers that, by the end of 2007, will include all of the eastern slopes of the Rocky Mountains from the Montana border to the provincial boundary of the Northwest Territories. The entire study area encompasses a mosaic of nearly 25 Landsat TM scenes, a product that is essentially impossible to duplicate at the same spatial

resolution annually or even bi-annually due to short growing seasons and persistent cloud cover in these areas (Wulder, 2004; Fraser *et al.*, 2005). Further, instruments such as those from Landsat Thematic Mapper or *Satellite Pour Observation de la Terre* (SPOT), that offer moderate or high spatial detail, typically have small swath widths and long repeat times that result in compositing intervals that are too large to resolve accurate time scales for many of these changes. As a result, the working maps are often out of date (i.e., based on most recent *best* available TM or ETM+ data), and there is dearth of alternative methods to update these products (McDermid *et al.*, 2005).

Coarser spatial resolution sensors (e.g., 250 to 1000 m) have the ability to overcome some of these limitations. For example, since 2000, the Moderate Resolution Imaging Spectroradiometer (MODIS) has been collecting data across the globe every one to two days. High quality, cloud free mosaics are produced at 16-day intervals and are presently available at no cost to the user. The spectral resolution ranges across 36 spectral bands from visible to thermal infrared (between 0.405 and 14.385 μm). Of the seven bands collected for land surface remote sensing, two are available at the 250 m resolution: Band 1 - Red: 620 to 670 nm and Band 2 - Near Infrared (NIR): 841 to 876 nm (Townshend *et al.*, 2002; Justice *et al.*, 2002). Research has suggested that these are among the most important spectral regions for remote sensing of vegetation, and interest is growing within MODIS-based, coarse resolution change detection studies (Coppin *et al.*, 2004; Fraser *et al.*, 2005). Phenomena have ranged from climate-driven phenology (Moody and Johnson, 2001), natural disturbances (Tansey *et al.*, 2004; Chuvieco *et al.*, 2005), and forest harvesting (Zhan *et al.*, 2002; Jin and Sader, 2005). Recent attempts use an assortment of change detection techniques including change metrics (Fraser *et al.*, 2005), iterative estimation (Le Hegarat-Masclé *et al.*, 2005), end-member and spectral signatures (Thenkabail *et al.*, 2005), logistic regression (Fraser *et al.*, 2003), decision trees (Zhan *et al.*, 2002), multi-date differencing (Kasischke and French, 1995), and supervised classification (Jin and Sader, 2005). Gitas *et al.* (2004) used an object-based classification to detect burned areas, however, in the literature, there are few multiple spatial resolution change detection studies that use an object-based combination of Landsat, 30 m data with coarser spatial resolution data like MODIS. Further, little research has focused on coarse resolution, satellite data for the purposes of supporting temporally accurate and spatially

Photogrammetric Engineering & Remote Sensing
Vol. 74, No. 8, August 2008, pp. 973–985.

Department of Geography, 9 Campus Drive,
University of Saskatchewan, Saskatoon, SK, S7N 5A5
(steven.franklin@usask.ca).

0099-1112/08/7408-0973/\$3.00/0
© 2008 American Society for Photogrammetry
and Remote Sensing

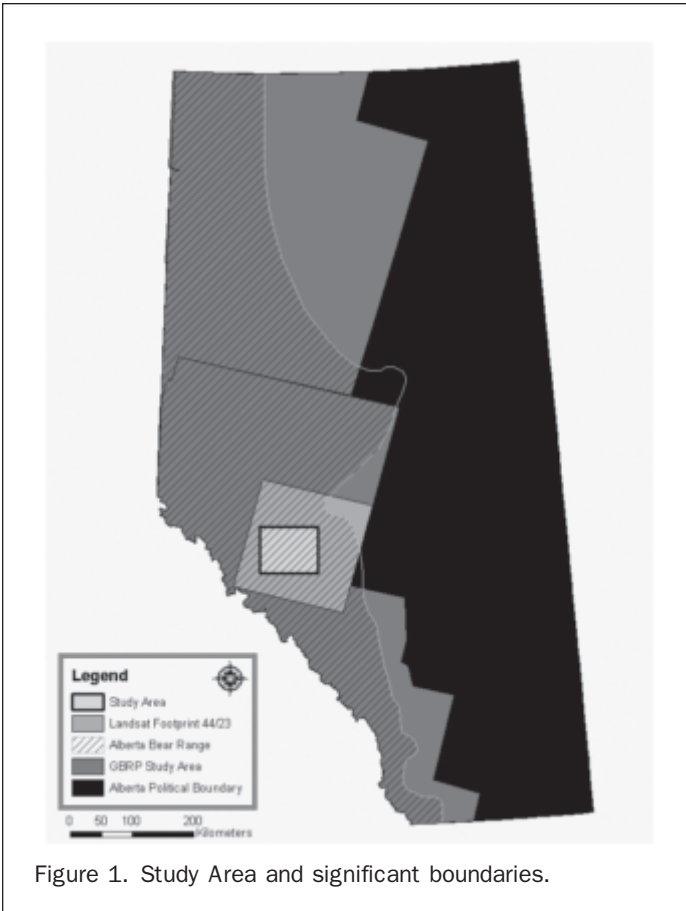


Figure 1. Study Area and significant boundaries.

Imagery Acquisition and Preprocessing

Landsat Data

Based on availability, cloud-free imagery consisting of a Landsat-7 Enhanced Thematic Mapper Plus (ETM+) image acquired 14 September 2001 and a Landsat-5 Thematic Mapper (TM) image acquired 17 September 2005 (Path/Row 44/23) were used to support the Landsat portion of the change detection study. The entire 2005 Landsat-5 TM image was radiometrically calibrated to convert digital number (DN) to radiance to at-satellite reflectance values consistent to those of Landsat-7 ETM+ using a Top of Atmosphere (TOA) Correction outlined by Chander and Markham (2003). In order to calculate the TOA reflectance values, the DN's are first converted to the original 32-bit radiance values measured by the sensor using the equation:

$$L_{\lambda} = Gain_{\lambda} * DN_{\lambda} + Bias_{\lambda} \quad (1)$$

where λ = TM band number, L_{λ} = at-satellite radiance, $Gain$ = band-specific gain obtained from the header file, and $Bias$ = band-specific bias, obtained from the header file.

Once the radiance values are calculated, the at-satellite reflectance is calculated as:

$$\rho = \frac{\pi * L_{\lambda} * d^2}{ESUN_{\lambda} * \sin(\theta)} \quad (2)$$

where λ = TM band number, L_{λ} = at-satellite radiance, ρ = TOA reflectance, $ESUN_{\lambda}$ = mean solar exoatmospheric irradiance, and θ = sun elevation angle, obtained from the header file.

In addition to the radiometric corrections, both 44/23 scenes were geometrically calibrated to eliminate relief displacement. To achieve this, each scene was orthorectified using the satellite orbital math model found in PCI Geomatica® OrthoEngine (Toutin, 1995). Ground control points ($n = 25$) were collected across the entire image using a 30 m DTMI digital elevation model (DEM) and a manually digitized, government-issued Roads layer. The Roads layer was created from orthophotos, high spatial resolution imagery, and ground data. It defines the standard geometric quality for all Landsat scenes used within the GBRP. In order to ensure precise registration, resulting second-order polynomial produced from this process requires a root mean square error (RMSE) of less than 0.5 pixels. Once this was achieved, the image data were resampled using a nearest neighbor algorithm to produce a 30 m grid projected to UTM Zone 11, NAD83 datum based on the GRS80 ellipsoid to ensure precise integration with other data in the GIS. Following visual inspection of geometric quality based on the Roads layer, clear cuts and other linear features, the data were clipped to the test area of 3,114 by 2,519 pixels covering a total area of 7062 km² (Figure 1).

The wetness index of the tasselled cap transformation was calculated for the at-satellite reflectance of both the Landsat-7 ETM+ (Crist and Cicone, 1984) and the Landsat-5 TM (Huang *et al.*, 2000) test area. This index was used to generate the Enhanced Wetness Difference Index (EWDI) based on the study by Franklin *et al.* (2001). Shown here are the Landsat TM coefficients, where LS_{Band}^* refers to the individual reflective Landsat bands:

$$Wetness = (0.2626 * LS_{Band1}) + (0.2141 * LS_{Band2}) + (0.0926 * LS_{Band3}) + (0.0656 * LS_{Band4}) + (-0.7629 * LS_{Band5}) + (-0.5388 * LS_{Band7}). \quad (3)$$

MODIS Data

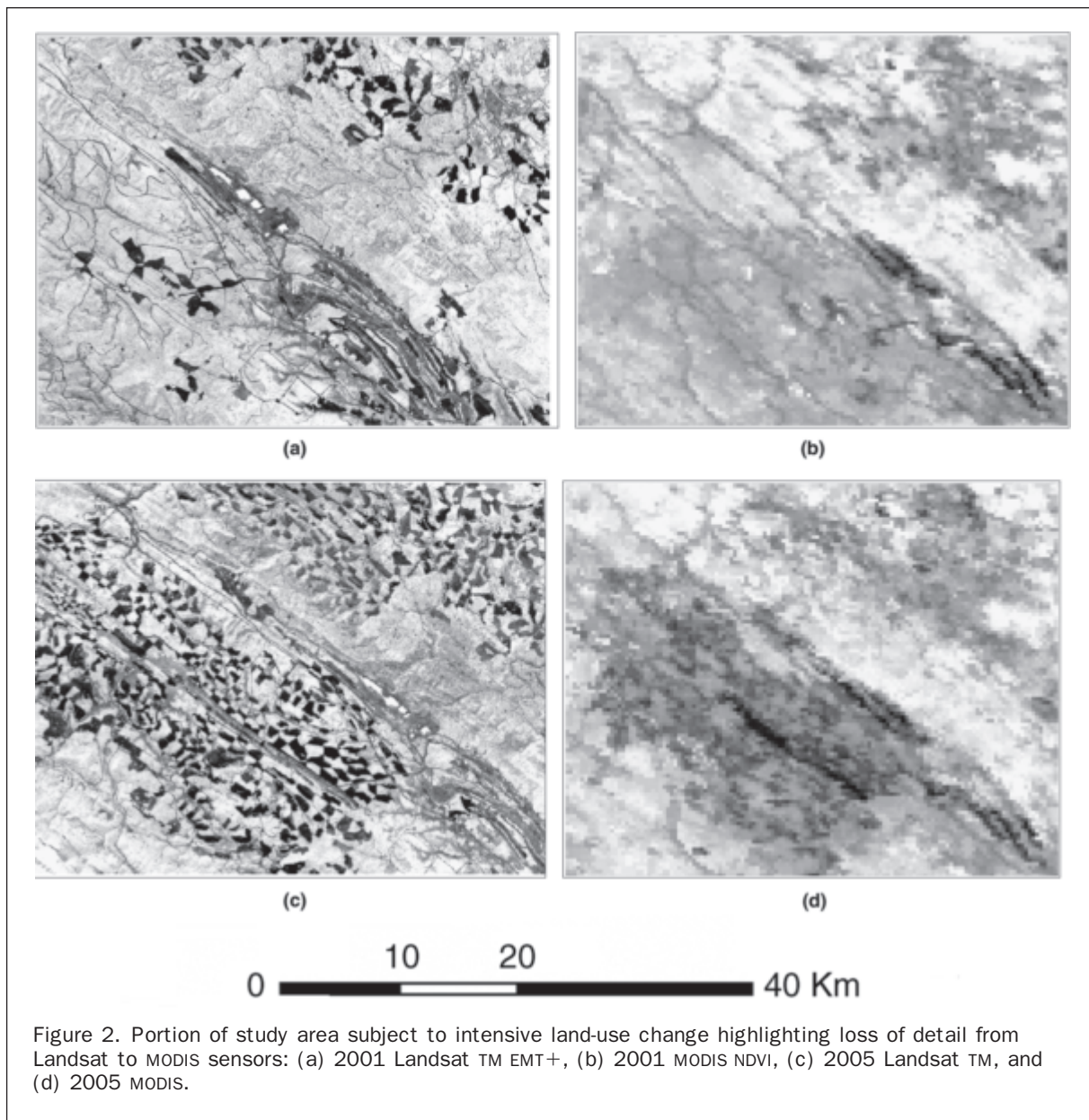
The MOD13Q1 product contains vegetation indices that were specifically designed to provide consistent spatial and temporal comparisons of global vegetation cover to support

adequate, large-area mapping and monitoring programs despite recent trends towards regional and global monitoring projects (Franklin, 2001; Olsen *et al.*, 2002; Wulder *et al.*, 2003; Wessels *et al.*, 2004; Stenhouse and Graham, 2005).

The objectives of this study are to (a) fill these gaps in the literature by evaluating the ability of a multiple scale, polygon-based dataset to detect forest disturbance, (b) to determine the patch size at which forest disturbances are accurately detectable with a multi-spatial, polygon-based dataset, and (c) to determine if and where such products can be used for the purpose of updating existing map products. A GIS-based (manual) change layer and a Landsat change detection layer will provide the reference data for validation and accuracy assessments.

Study Area

The study area is located in a boreal forest along the eastern slopes of the Rocky Mountains near Hinton, Alberta, Canada in a moderate to high elevation within the existing Grizzly Bear Research Program (GBRP) study area. The area covers a subset of Landsat Path/Row 44/23 and encompasses more than 7,000 square kilometers (Figure 1). This prime Grizzly Bear habitat is composed of mixed and pure stands consisting primarily of white spruce (*Picea glauca*), lodgepole pine (*Pinus contorta*), and trembling aspen (*Populus tremuloides*) (Stenhouse and Graham, 2005). Extensive land-use activities occurring in this area (for example, oil and gas exploration and forestry) will provide practical examples of change at different spatial scales that are likely to occur within similar forest types (Figure 2).



change detection and phenological studies (Justice *et al.*, 2002; Jin and Sader, 2005). Contained in tile 10v03, all available, MOD13Q1 scenes from summer (July to early-September) 2000 to 2005 were downloaded from the MODIS website (<http://edcimswww.cr.usgs.gov/pub/imswelcome/>), but only six composite dates were selected based on availability of nearly cloud-free data that correspond with the Landsat acquisition dates as outlined in Table 1. MODIS products are atmospherically corrected before release

TABLE 1. SATELLITE IMAGERY ACQUISITION DATES

Year	MODIS	Landsat
2000	28 August	
2001	13 August	14 September
2002	29 July	
2003	13 August	
2004	13 August	
2005	28 July	17 September

therefore, preprocessing was limited to: (a) reprojecting the sinusoidal projection to UTM Zone 11 (NAD 83), (b) translating the dataset to a usable file format, and, (c) clipping the mosaic to fit the study area. These tasks were completed using the MODIS Reprojection Tool downloaded from the NASA Land Processes Distributed Active Archive Center. In total, six image dates were selected to create two different change products: (a) a five-year composite of annual change layers, and (b) a five-year, two-date change layer.

Manual GIS Change Layer (Δ GIS)

A reference change layer (called Δ GIS) was compiled based on existing clear-cut and well-site data stored in the FMF GBRP data archive. To create Δ GIS, existing cut-block and well-site data were available over nearly 85 percent of the area. Image interpretation and manual digitization of aerial photographs and high-resolution SPOT5 imagery (acquired July 2005) provided additional change features, and finally, the 2005 Landsat TM image was used to digitize any remaining change

features (less than 10 percent). Features such as roads, well-sites, and clear-cuts were readily identified through multiple field observations designed to identify each change mapped in the GIS database. These field observations were acquired by interdisciplinary field teams assembled for the purpose of training data acquisition and verification of the land-cover classification. Typically, manual interpretation of change is confirmed in the form of experience and/or ancillary data which include other classification maps, Geographic Information Systems (GIS) layers, ground truth data, and aerial photography. Despite minimal error associated to change omission, the GIS-based change layer (Δ_{GIS}) was used as the validation layer for the study.

Landsat-Based Polygon Layer

The polygon layer used in this study was clipped from the 2003 GBRP Land-cover Map (McDermid *et al.*, 2005). The layer was created from 30 m Landsat data using the Multiresolution Segmentation algorithm provided in Definiens® Professional 5.0 (formerly eCognition® 4.0). This algorithm creates larger objects through a clustering process based on weighted heterogeneity. The size of each polygon is controlled by user defined parameters for weight, scale, and shape parameter (McDermid *et al.*, 2005). To create the polygon layer used for this study, various combinations of input variables and parameters were tested to ensure all landscape features were appropriately represented. The combination ultimately used was based on a blend of the tasseled cap variables brightness, greenness, and wetness (weight 1.0), and the DEM derivatives of slope and incidence (weight 0.3). The scale parameter was set to 9, and the composition criteria were color: 0.8, shape: 0.2, smoothness: 0.8, and compactness: 0.2. Average polygon sizes are outlined in Table 2.

Image Differencing Methods

A series of one-year and five-year change maps were created using the 2000 to 2005 imagery to create the polygon-based change detection layers for comparison, several steps were required. First, the MODIS NDVI values were applied to the polygon layer using the VIMAGE algorithm in PCI Geomatica®'s Algorithm Library. This algorithm applied the mean value of the NDVI pixels found within each polygon to create a multiple spatial resolution, polygon-based layer of average mean NDVI MODIS values (Figure 3). Next, the polygon-based, NDVI layers were subtracted (YEAR 1 – YEAR 2) resulting in six separate layers of Change/No-Change: one two-date, multi-year change layer from 2000 to 2005 (Δ_{SM}), and five annual change layers that were merged to produce one five-year multi-date composite of Change (Δ_{CM}).

Following the creation of the Change products, the next step, and one of the most crucial was thresholding

i.e., determining the value(s) of actual change instead of differences that may be a result of sensor noise, atmospheric differences, geometric error, or other non-land-cover change source. For this process, earlier work by Franklin *et al.* (2005) suggested that selecting a threshold of two standard deviations from the mean (i.e., mean difference in pixels in change polygons) resulted in appropriate change threshold for Landsat TM or ETM+ Enhanced Wetness Difference Index studies of forest canopies. Visual inspection of the resulting *thresholded* imagery suggested that this was an adequate reference point for this MODIS study however, manual adjustments were necessary to generate optimal threshold values for the changes to be mapped.

These steps were repeated with the Landsat EWDI to create the polygon-based Δ_{TM} . Upon completion of the final change layers, several accuracy and map comparison tests were performed to evaluate the quality of the MODIS change detection at different spatial scales (or patch size) as compared to the GIS-based change layer (Δ_{GIS}) and the Landsat EWDI change detection (Δ_{TM}) of the same area.

Accuracy Assessment

Creating the sampling strategy for assessment points posed a challenge and therefore, several sampling strategies were implemented for the accuracy assessment. First, a proportional sample was selected; i.e., a random selection of polygons was generated. This resulted in extremely high accuracies overall due to the mis-proportion of Change:No-Change (4:96). For example, too much of the image had not changed, and a direct proportional sample was biased to those no-change areas. The accuracy of the Change class was of primary interest in this study (i.e., the occurrence of omission error was thought to be of greater consequence), so it was important to ensure the number of points representing “No-Change” did not falsely improve the overall map accuracy. In order to represent all types of change within the area, one training point was assigned to each change polygon contained within Δ_{GIS} polygon ($n = 1,418$). No-Change points ($n = 400$) were randomly generated within Δ_{GIS} . This sample size was chosen based on a study by Congalton (1991) who suggested that increasing sample size beyond this point does not significantly effect the final statistics. To avoid the effects of mixed-pixels and confusion along edges, especially within the coarse resolution pixels, each of the No-Change points was placed at least 400 m from the edge of change polygons (equivalent to approximately 1.5 MODIS pixels).

Using the sample points, both validity and reliability were assessed. First, validity (the agreement between the value of a measurement and its true value on the ground) was tested using a confusion matrix for each Δ_{CM} , Δ_{SM} , and Δ_{TM} with the reference map Δ_{GIS} . The matrix was then used to determine the overall map accuracy, error of omission, and error of commission. Next, reliability (or the reproducibility of the maps) was assessed by calculating KAPPA:

$$k = \frac{\pi_o - \pi_e}{1 - \pi_e} \quad (4)$$

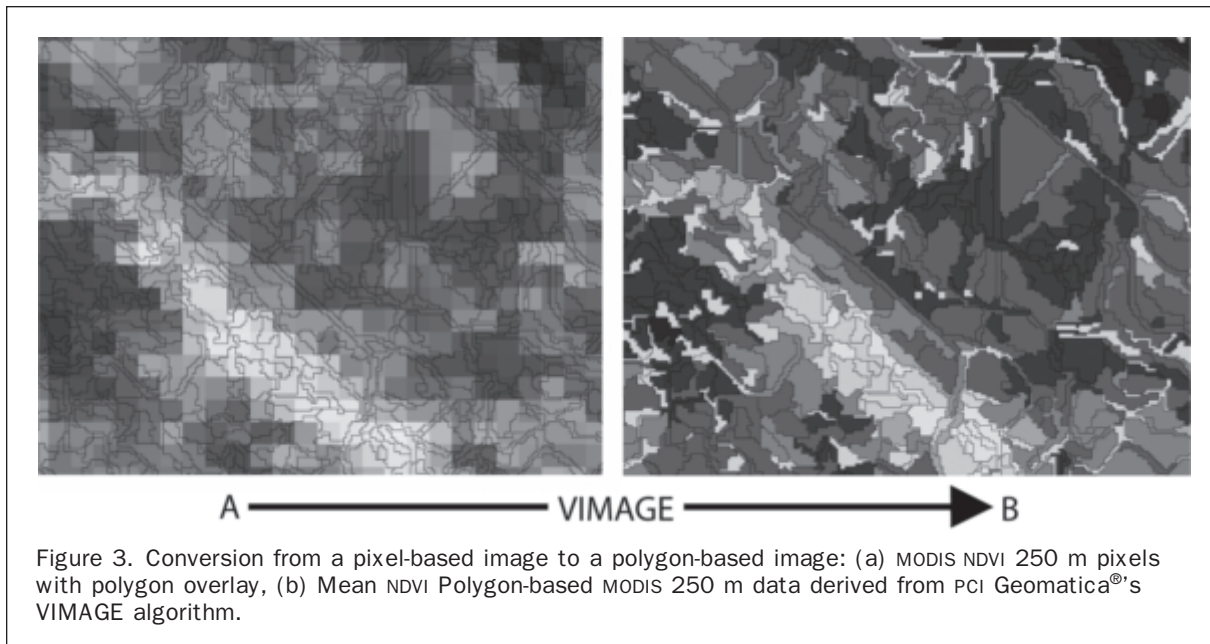
where π_e = expected probability of agreement, and π_o = actual agreement.

The KAPPA calculation produces an index that compares agreement with chance and can be thought of as the chance-corrected proportional agreement. Possible values range from +1 (perfect agreement) to 0 (no agreement above that expected by chance) to -1 (complete disagreement). Landis and Koch (1977) suggest the following for one possible interpretation of KAPPA:

- Poor agreement = Less than 0.20
- Fair agreement = 0.20 to 0.40

TABLE 2. SIZE DISTRIBUTION OF POLYGONS IN LANDSAT TM SEGMENTATION

Size (Ha)	Number of Polygons
0–2	20,681
2–4	35,034
4–6	26,447
6–8	17,242
8–10	10,638
10–15	10,880
15–20	3,257
20–25	1,053
25+	631
Total	125,863



- Moderate agreement = 0.40 to 0.60
- Good agreement = 0.60 to 0.80
- Very good agreement = 0.80 to 1.00.

In addition to the accuracy assessments mentioned above, a map classification comparison was performed providing insight into how the actual spatial coverage of change polygons (ΔSM and ΔTM) compare to polygons of ground data (ΔGIS). This assessment provided a different perspective on the accuracy because (a) information concerning the association among specific individual classes in a confusion matrix can be lost by summary association measures, and (b) this test provided a spatially explicit comparison.

Next, the Cramer's V correlation coefficient (V) was calculated. A statistical correlation coefficient such as this is used to measure the relationship between two categorical variables and represents this association with values ranging from 0 (no association) to 1 (perfect association) (Davis, 1986). Additionally, the Cramer's V statistic is not affected by sample size, and therefore is very useful in situations where one may suspect a statistical significance was the result of a large sample size instead of any substantive relationship between the variables. For example, one study by Klita *et al.* (1998) compared AVHRR and Landsat TM classifications of a boreal forest in Northwest Alberta using the Cramer's V. One other comparative study by Fosnight and Fowler (2001) used this statistic to compare an AVHRR-based U.S. Land Cover Characterization and a photo-based USGS Land-cover and Land-use map. The AVHRR data were scaled to match the spatial scale of this classification and cross tabulation from the two differing datasets tested several measures of association and agreement. For rectangular cross classified tables, the Cramer's V performed in the top three and authors suggested that it be used as a test of independence between two classifications (Fosnight and Fowler, 1996). It is calculated as:

$$V = ((X^2/N(L - 1))^{1/2} \quad (5)$$

where X^2 = Chi Square, N = the total number of observations in the contingency table, and L = the minimum number of rows or columns in the contingency table.

Natural Breaks Classification

As mentioned above, several authors have used MODIS for the purpose of detecting forest disturbance, and the general consensus is that smaller forest disturbances are not accurately detected with 250 m MODIS data. One study by Jin and Sader (2005), did find that patch size greater than 20 hectares will be detected by a supervised classification of MODIS NDVI data with an accuracy of 75 percent or higher in a temperate forest suggesting that a fourth test is necessary to determine the minimum polygon size for change to be accurately identified using the multi-spatial resolution method. To achieve this, polygons and their associated validation points from ΔGIS were distributed into 13 size classes based on natural breaks within the data. This dataset was subject to the KAPPA and error matrix accuracy tests and size classes are summarized in Figure 4.

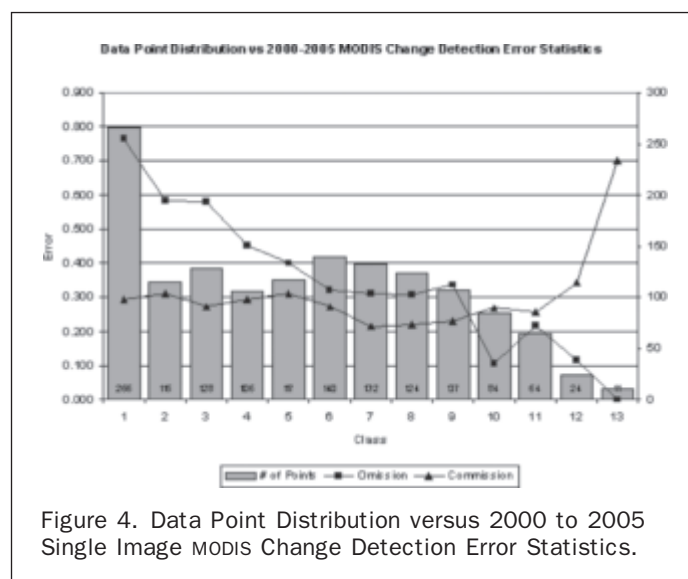


Figure 4. Data Point Distribution versus 2000 to 2005 Single Image MODIS Change Detection Error Statistics.

Results and Discussion

The results of the change detections are displayed in Figure 5. The results of the error matrix (Tables 3 and 4) showed that the single-image MODIS change detection, Δ_{SM} , provided the best results (59 percent overall accuracy, KAPPA 0.272), possibly because of cumulative data problems (e.g., atmospheric effects) in comparing imagery year-by-year over the five-year interval in Δ_{CM} (52 percent overall accuracy, KAPPA 0.199). Also, it is possible that some of the first forest clearcuts were created shortly after initial image acquisition and were maturing by the time of sequential image collection resulting in weaker spectral changes (Lunetta *et al.*, 2004). The TM-based procedure yielded approximately 85 percent accuracy with a KAPPA of 0.638 which is consistent with the results of other EWDI studies. Spatial representation of the changes detected by MODIS and Landsat agree generally with those mapped in the Δ_{GIS} (Figure 5a). The general pattern of change is apparent through the Δ_{TM} (Figure 5c) and Δ_{CM} and Δ_{SM} (Figure 5b and Figure 5d, respectively) however, Δ_{CM} appears to contain more errors of omission and commission.

Closer inspection of a small area reveals some interesting details in the change detection output (refer to Plate 1). Significant omission is apparent (see Plate 1 identified with

the number 1 in the top central part of the upper right image map); here, the GIS contained a large polygon identified as change which was not captured in either of the MODIS change detection procedures. In the lower portion of the Plate (lower central, labeled as the number 2), partial change detection appears to have occurred; here, the GIS data suggest several polygons were missed, but that others were quite accurately identified in the MODIS procedure. And finally, in the lower right hand side of the Plate (labeled as number 3), very accurate change detection appears to have occurred, since the GIS polygons appear to overlay almost perfectly the change polygons identified in the MODIS image differencing.

Map Agreement Comparison

The map agreement comparison spatially compared each of Δ_{SM} and Δ_{TM} to the control, Δ_{GIS} . These are displayed in Plate 2. The largest difference was found between Δ_{SM} and Δ_{GIS} (Table 5), however, the statistics show that Δ_{SM} was able to detect over half of the changes (54 percent) included in the Δ_{GIS} and 96 percent of the total No-Change included in Δ_{GIS} . Δ_{SM} included an additional 3.79 percent and missed 1.42 percent of overall change compared to that of Δ_{GIS} .

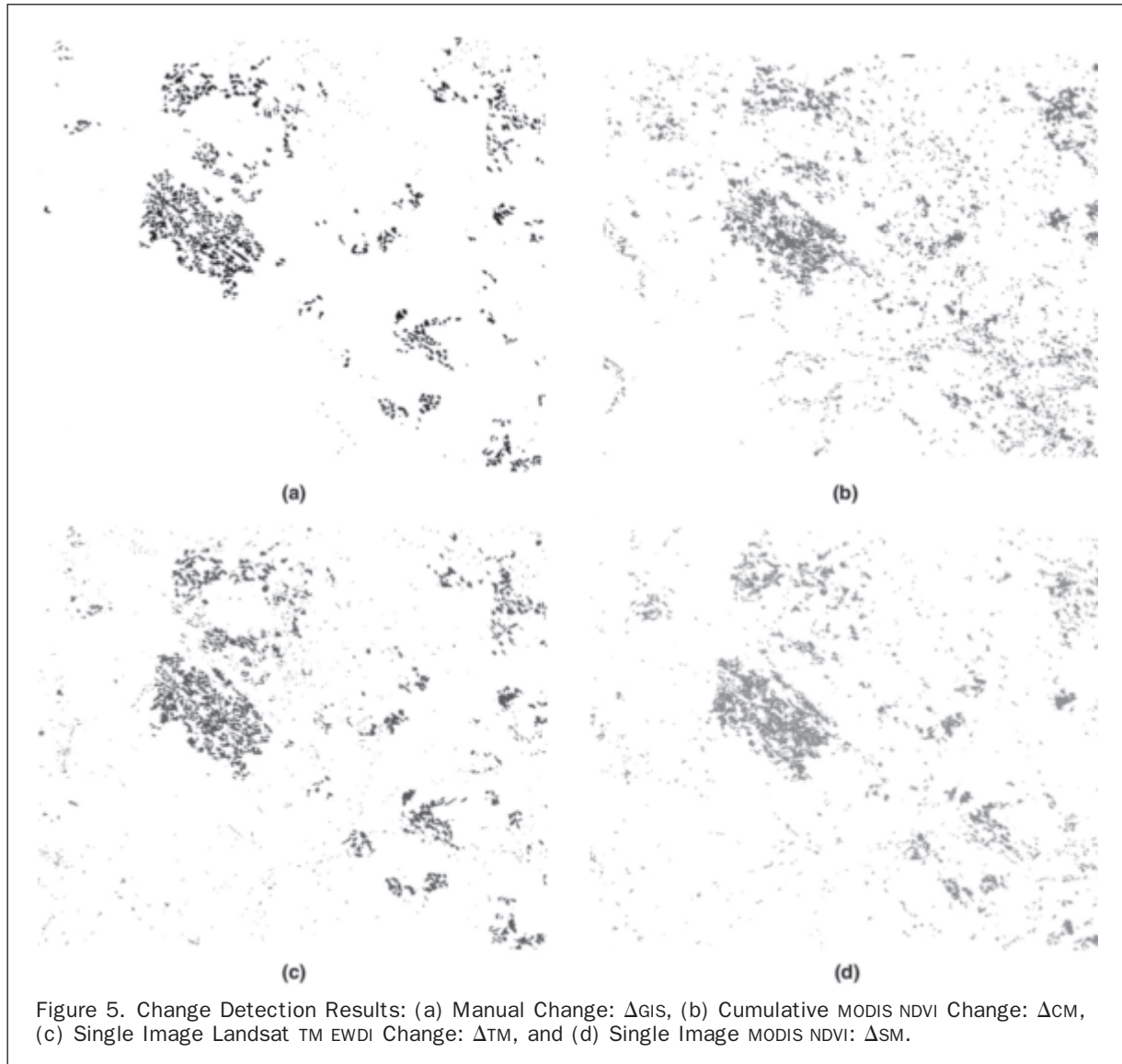


Figure 5. Change Detection Results: (a) Manual Change: Δ_{GIS} , (b) Cumulative MODIS NDVI Change: Δ_{CM} , (c) Single Image Landsat TM EWDI Change: Δ_{TM} , and (d) Single Image MODIS NDVI: Δ_{SM} .

TABLE 3. RESULTS OF THE ERROR MATRIX

	No-Change	Change	Total	% Correct	% Commission
Δ_{CM}					
No-Change	391	852	1231	30.8	68.5
Change	9	566	587	96.4	1.6
Total	400	1418	1818		
% Correct	97.8	39.9		51.98	κ
% Omission	2.3	60.1			0.199
Δ_{SM}					
No-Change	379	717	1096	34.6	65.4
Change	21	701	722	97.1	2.9
Total	400	1418	1818		
% Correct	94.8	49.4		59.4	κ
% Omission	5.2	50.6			0.272
Δ_{TM}					
No-Change	394	274	668	59.0	41.0
Change	6	1144	1150	99.5	0.5
Total	400	1418	1818		
% Correct	98.5	80.7		84.6	κ
% Omission	1.5	19.3			0.64

TABLE 4. ACCURACY AND ERROR MATRIX DESCRIPTIVE STATISTICS

Layer	Map Accuracy	Kappa	Change Error of Omission	Change Error of Commission
Δ_{SM}	0.594 (+/-0.041)	0.272 (+/-0.040)	0.506 (+/-0.027)	0.0291 (+/-0.013)
Δ_{CM}	0.520 (+/-0.065)	0.199 (+/-0.039)	0.601 (+/-0.026)	0.0358 (+/-0.016)
Δ_{TM}	0.846 (+/-0.017)	0.638 (+/-0.039)	0.193 (+/-0.021)	0.00522 (+/-0.0046)

Obviously, the larger pixel size of the MODIS data has created a similar area of change even though the number of change locations has been reduced (omitted). Comparatively, Δ_{TM} was able to detect 83.87 percent of the total change and 97.84 percent total No-Change found within the Δ_{GIS} layer. It still is not able to detect perfectly 100 percent of the change that was found by manual interpretation and GIS data layers, however, there is only a discrepancy of 2.6 percent across the entire area, i.e., less than half of the error associated with the Δ_{SM} .

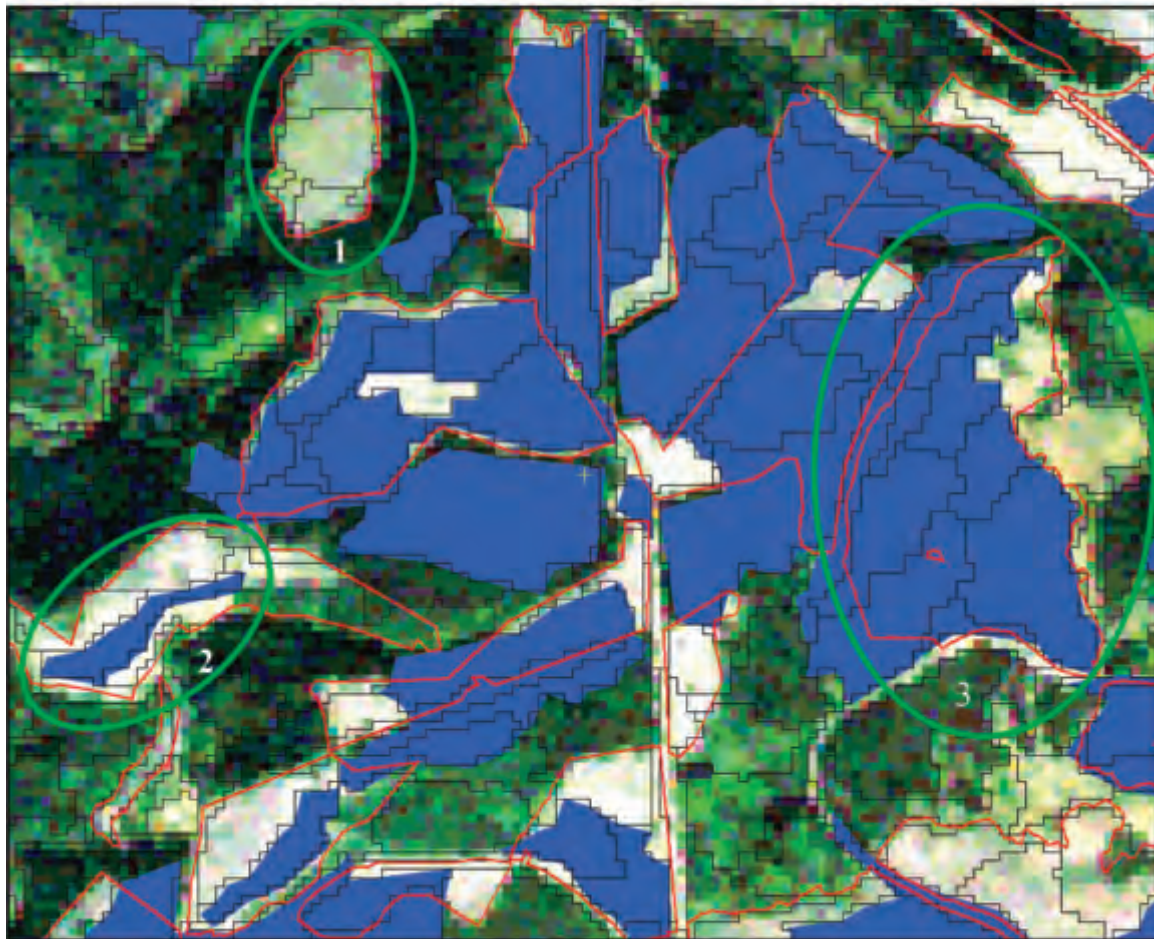
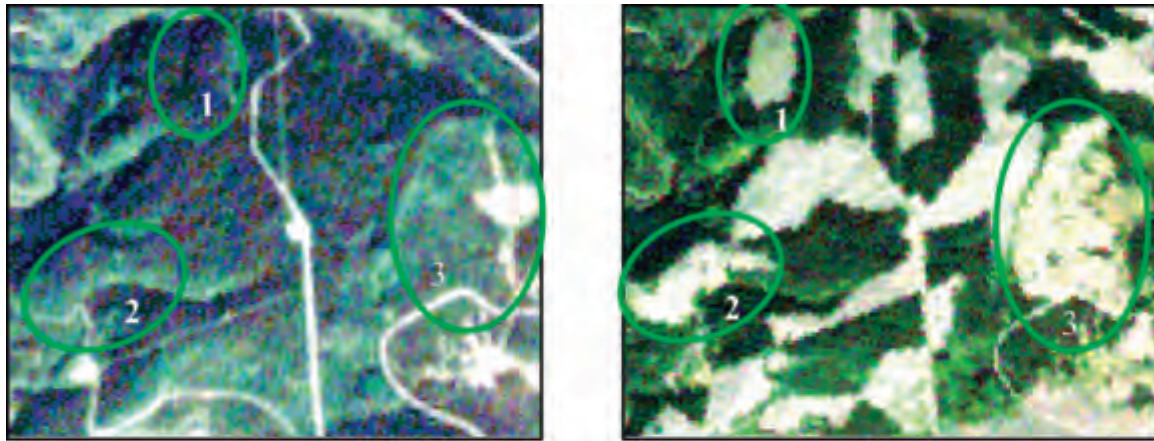
Cramer's V and the Contingency Coefficient (C)

The results of the Map Agreement Comparison, Cramer's V, and Contingency Coefficient are displayed in Table 5. Cramer's V values show significant agreement between the Δ_{SM} and Δ_{TM} with Δ_{GIS} , 0.38 and 0.67, respectively. This value is fairly low for the MODIS detection and closer to no association (Cramer's V = 0) than to complete association (Cramer's V = 1.00). However, if Δ_{TM} is normally accepted as the best replacement to Δ_{GIS} , (Cramer's V = 1.00), a different interpretation is that the maximum Cramer's V is 0.67 instead of 1.00. This indicates that the association is more likely 0.38 out of a possible 0.67 resulting in a "weighted" Cramer's V of 0.57.

Natural Breaks Classification

As anticipated, there is an increasing trend in the overall change class accuracy based on MODIS data with increasing polygon size (Figure 4). The error of omission decreases consistently to 0 percent in the classification for the largest size class; the smallest size class is the least accurate as expected. The error of omission appears to level off to approximately 0.21 with size classes 6 and 7 (14.5 to 19.2 hectares and 19.2 to 24.5 hectares); one interpretation

of these results is that change polygons of approximately 15 hectares in area may be the optimal size for successful detection of change features using MODIS data. At this point, the error of commission also decreases slightly, at least until Class 7, at which point the error of commission does increase slightly. Unfortunately, this is the point in the sample at which the number of training data within each class is quite low, and therefore, this could have significantly affected the error of omission associated with the No-Change class. In an attempt to overcome this problem, the original segmentation used for the change detections was used to apply a size class to each of the 400 No-Change points. This did improve the results for all map agreement tests, however, the overall trend did not change as expected. One reason may be that the polygons within the segmentation do not match perfectly with Δ_{GIS} , and therefore, the overall area of change is affected (Figure 6). Secondly, since the scale parameter of the segmentation was preset to 9, this effectively limits the representation within the larger size classes (Table 2); for example, for class 13 (polygons over 10 hectares), $n = 5$, and even small differences have large impacts on the results. Plate 3 suggests one additional problem when applying coarser satellite resolution data sets to a polygon based map update. The GIS polygons are shown in red, and the underlying polygons are those mapped using the segmentation procedure on the original Landsat imagery; clearly, there are major questions associated with the appropriateness of the Landsat-based polygons as *identifiable* features when the GIS polygons are mapped as change. This problem is made even more difficult to resolve when the larger pixel sizes of the MODIS data set are incorporated in the change update. In summary, however, the users of the map are most interested in overall accuracy on the ground, and therefore, would likely prefer to use Δ_{GIS} as the reference map when available.



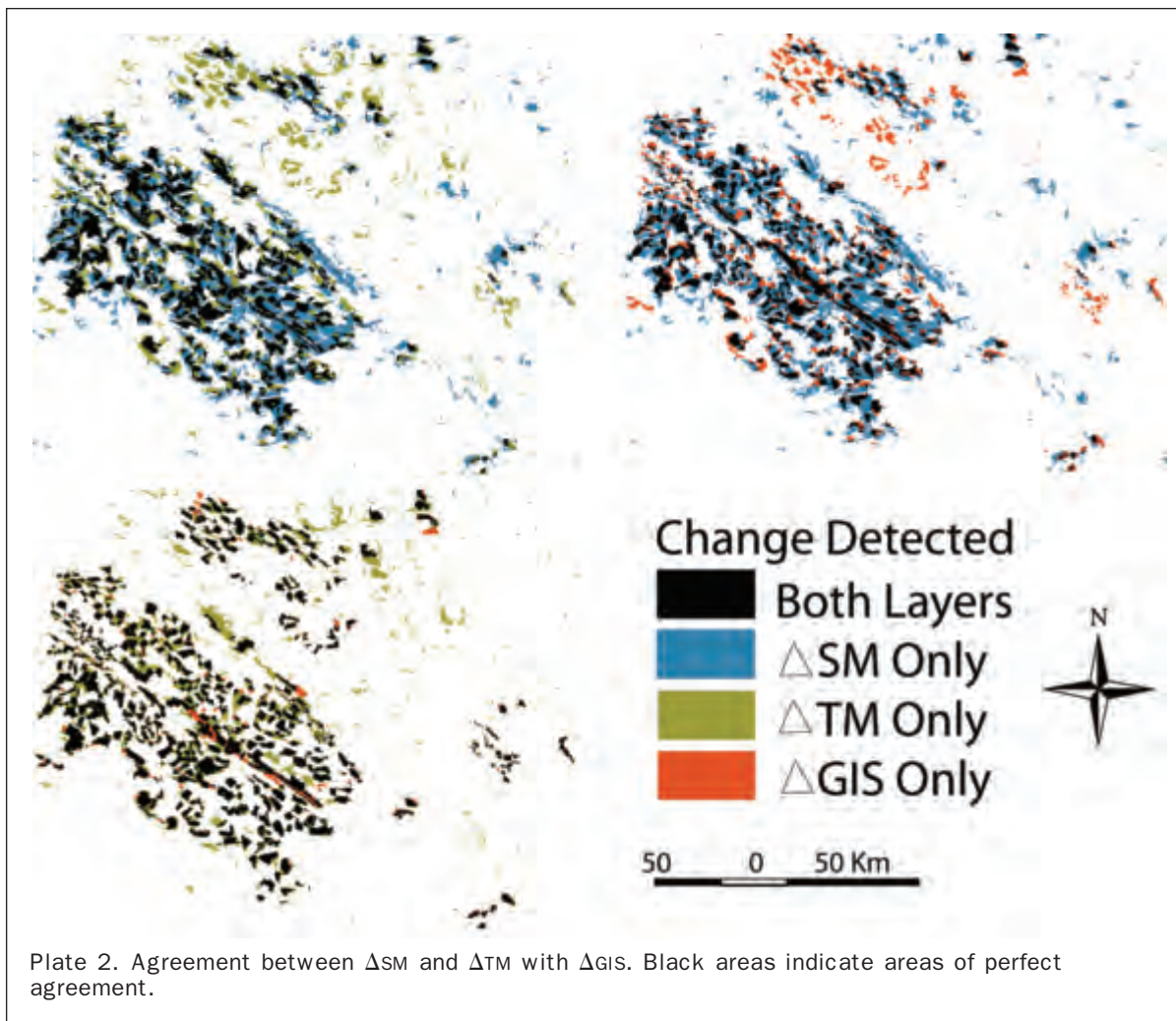
- Area of Interest
- Δ GIS
- Δ SM

Plate 1. An example of change detected within Δ SM compared to 2001 Landsat-7 ETM+ and 2005 Landsat-5 TM. Highlighted areas include: (1) No-Change detected, (2) partial Change detected, and (3) almost perfect Change detected.

Pixel Size, Pixel Location, and Thresholding Issues

When using different spatial resolution data sets, pixel size and location are important mapping challenges. Plate 4 shows examples of this; when the pixel size is different in

the update imagery, there can be new *blockiness* introduced into the final update map product that may reduce user confidence and applicability. The pixel location problem suggests that the segmentation in the original land-cover



map may not be optimal for the update process; in other words, there can be a difference between the areas identified as change in the imagery and the available segments that need to be updated. Some decisions might be required that have little in the way of practical guidance to support them, and, again, user confidence and map applications may be compromised. Additionally, these figures display the challenges associated with polygon size and shape, again, a characteristic of the final map that is dependent on the original, segmented land-cover product.

Thresholding has long been an issue within satellite imagery change detection studies, and the present study is

no exception; the results presented here are very sensitive to the selection of the threshold, as the mapper is trying to balance the detection of *too much change* versus missing actual change features on the ground. The ability to select an appropriate threshold of change to exclude undesired *noise* determines the success of the change detection. Typical methods are based on qualitative choices, for example, airphoto interpretation (Mas, 1999), field methods, and individual expertise (Lyon *et al.*, 1998). Few studies are available within the literature that use more quantitative methods; it is possible that higher overall accuracy in the MODIS change detection procedures could be obtained with a

TABLE 5. RESULTS OF THE MAP AGREEMENT COMPARISON (PERCENT AREA) AND CRAMER'S V

	Percent Area of Study Area			
	Δ_{GIS}^{**} vs. Δ_{TM}^*	Δ_{GIS}^{**} vs. Δ_{SM}^*	Δ_{SM}^{**} vs. Δ_{TM}^*	Δ_{GIS}
"NO-CHANGE" AGREEMENT	94.81	93.1	92.17	96.9
"CHANGE" AGREEMENT	2.6	1.68	2.33	3.1
DATASET 2** "CHANGE" MISSED BY DATASET 1*	0.51	1.42	3.15	
DATASET 1* "CHANGE" MISSED BY DATASET 2**	2.09	3.79	2.36	
CRAMER'S V	0.670	0.383	0.431	



Figure 6. Partial detection due to ΔGIS polygon centroid location: (A) shows agreement between ΔSM and the accuracy point, and (B) is an example where change was partially detected within ΔSM , however, the location of the centroid in this polygon is outside of the change area and therefore excluded in the accuracy assessment.

different thresholding technique. One suggestion for future studies is an automated binary change detection model recently created by Im *et al.* (2007). This model calibrates multiple user input variables for continuous thresholds and produces graphs that assist the users' understanding of patterns between threshold and accuracy, at the same time, removing the noise and false positives in an efficient manner (Im *et al.*, 2007). These models show promise for improving the accuracy of detecting forest disturbance, even possibly among polygons less than 15 hectares; however, the results presented here are internally consistent since the same two-standard deviation threshold was applied in all change layer procedures.

Conclusions

The main objectives of this study were to detect forest disturbance using a multiple spatial resolution, polygon-based method and to determine the minimum patch size at which these changes can be accurately detected. Quantitative data on MODIS change detection, the multiple spatial resolution method, and patch size provides a better understanding of the potential for MODIS to be used in updating existing map products for use in grizzly bear studies and

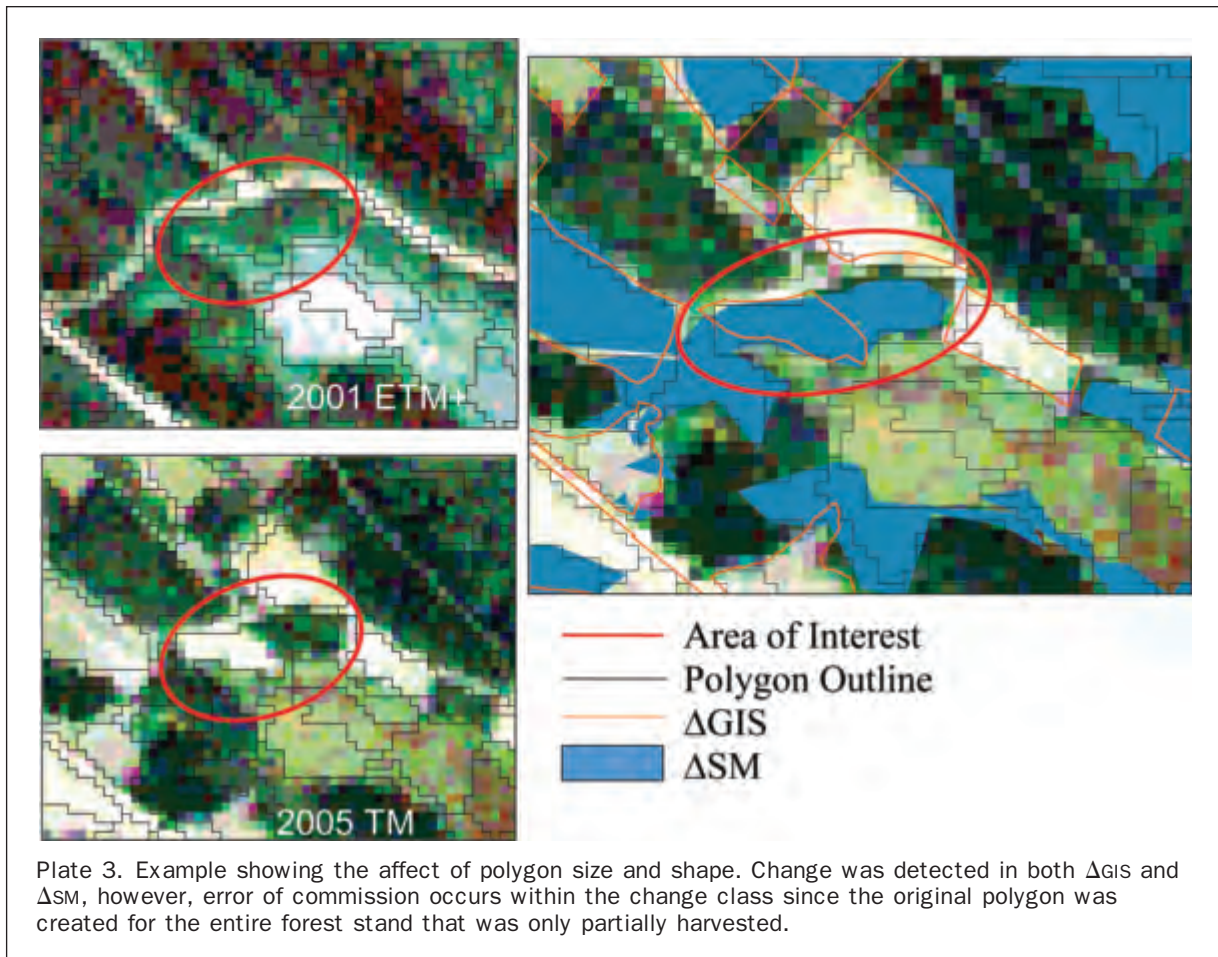
monitoring of other regional or global areas. Overall, the MODIS sensor performed reasonably well considering the spatial resolution is less than eight times that of Landsat TM; the greatest sources of error reported were the relatively large omission errors in small change polygons. Changes greater than 15 hectares were detected accurately, thereby providing a basis for further research and identifying areas where higher spatial resolution imagery are required. The results suggest that because smaller changes are not reliably detected by the MODIS sensor, the map updates presented here are probably appropriate in some but possibly not all wildlife studies. However, despite the significant amount of detail and information not present when these data are compared to Landsat or SPOT sensor data, using coarse resolution data are clearly better than doing nothing and using an *outdated* map. For example, landscape fragmentation analysis may be reasonable when the landscape metrics are calculated using MODIS-based change detection maps. More research on the impact of different mapping products on this landscape fragmentation and other wildlife applications may be useful in future.

Also, it is important to note that these results are based on only the "first" layer of data and no additional layers (that may be available with some MODIS products) were utilized to assess whether or not some sort of radiometric normalization of MODIS datasets may improve the overall results of image differencing. In the study by Fraser *et al.* (2005), a Thiel-Sen regression applied to MODIS imagery proved to be effective in normalizing the broad-scale reflectance variations across Canada (their study area was the entire country). Additional studies that focus on this aspect will determine how to account for the error associated with radiometric, atmospheric, and topographic differences; further work may be required in those areas of change that are the result of differences in phenology (seasonal vegetation models, for example).

Furthermore, much of remote sensing science is moving towards mapping methods that are comprised of more polygon-based methods; therefore, research into the various polygonal issues should be investigated, including the original land-cover mapping specifications in the segmentation approach. More broadly, developing a rough guideline that provides information regarding optimal scale values for the derivation of specific land-use or land-cover features across the landscape may significantly improve the results of any mapping effort, and would have been of great value in this study. The general idea is that change detection methods can be *tailored* if there is a known relationship between the information content of the imagery and the type of changes that occur in the environment that is to be mapped; this would enable a more thorough multiple-scale approach to be implemented in which different parts of the mapping region are mapped for updates with different sources of data.

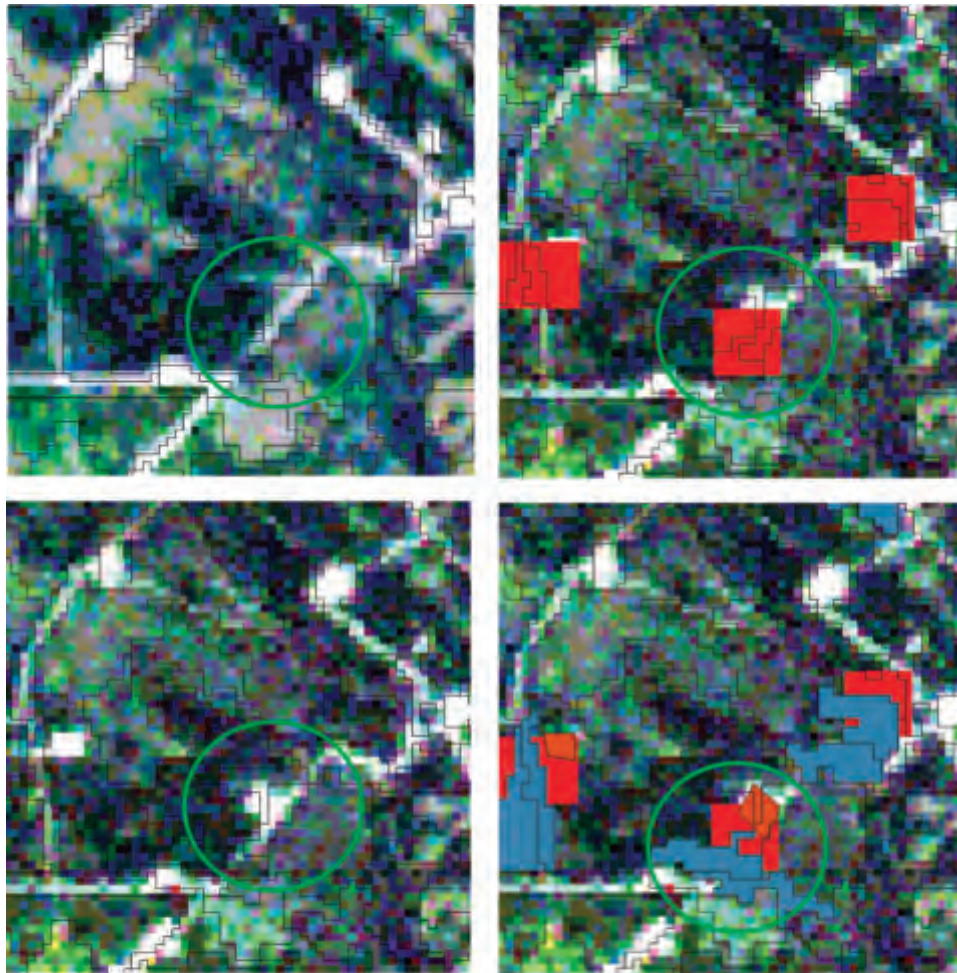
Acknowledgments

This research was funded by the Natural Sciences and Engineering Research Council of Canada and the Foothills Model Forest (Grizzly Bear Research Program) through a collaborative research and development grant. The MODIS data are distributed by the Land Processes Distributed Active Archive Center, located at the U.S. Geological Survey Center for Earth Resources Observation and Science (<http://LPDAAC.usgs.gov>). The authors gratefully acknowledge the GBRP Research team and all other collaborators specifically, Ame L. Wunderle, Dr. Greg J. McDermid, Dr. Marc Cattet, and Dr. Xulin Guo for their support, discussions, and expert advice.



References

- Chander, G., and B. Markham, 2003. *Revised Landsat TM Radiometric Calibration Procedures and Post-Calibration Dynamic Ranges*, United States Geological Survey publication, URL: http://landsat7.usgs.gov/documents/LANDSAT_5_TMTM_Cal2003.pdf (last date accessed: 12 March 2008).
- Chuvieco, E., G. Ventura, M. Martin, and I. Gomez, 2005. Assessment of multitemporal compositing techniques of MODIS and AVHRR images for burned land mapping, *Remote Sensing of Environment*, 94(4):450–462.
- Congalton, R.G., 1991. A review of assessing the accuracy of classifications of remotely sensed data, *Remote Sensing of Environment*, 37:35–46.
- Coppin, J., I. Jonckheere, K. Nackaerts, and B. Muys, 2004. Digital change detection methods in ecosystem monitoring: A review, *International Journal of Remote Sensing*, 10:1565–1596.
- Crist, E.P., and R.C. Cicone, 1984. Application of the Tasseled Cap concept to simulated Thematic Mapper data, *Photogrammetric Engineering & Remote Sensing*, 50(3):343–352.
- Franklin, S.E., 2001. *Remote Sensing for Sustainable Forest Management*, Lewis Publishers, Boca Raton, Florida.
- Franklin, S.E., C.B. Jagielko, and M.B. Lavigne, 2005. Sensitivity of the Landsat enhanced wetness difference index (EWDI) to temporal resolution, *Canadian Journal of Remote Sensing*, 31(2):149–152.
- Franklin, S.E., M.B. Lavigne, M.A. Wulder, and G.B. Stenhouse, 2002. Changed detection and landscape structure mapping using remote sensing, *The Forestry Chronicle*, 78(5):618–625.
- Franklin, S.E., and M.A. Wulder, 2002. Remote sensing methods in medium spatial resolution satellite data land cover classification of large areas, *Progress in Physical Geography*, 26(2):173–205.
- Franklin, S.E., M.B. Lavigne, L.M. Moskal, M.A. Wulder, and T.M. McCaffrey, 2001. Interpretation of forest harvest conditions in New Brunswick using Landsat TM Enhanced Wetness Difference Imagery (EWDI), *Canadian Journal of Remote Sensing*, 27:118–128.
- Fraser, R.H., A. Abuelgasim, and R. Latifovic, 2005. A method for detecting large-scale forest cover change using coarse spatial resolution imagery, *Remote Sensing of Environment*, 95(4):414–427.
- Fraser, R.H., R. Fernandes, and R. Latifovic, 2003. Multi-temporal mapping of burned forest over Canada using satellite-based change metrics, *Geocarto International*, 18(2):37–47.
- Gitas, I.Z., G.H. Mitri, and G. Ventura, 2004. Object-based classification for burned area mapping of Creus Cape, Spain, using NOAA-AVHRR imagery, *Remote Sensing of Environment*, 92(3):409–413.
- Gong, P., and B. Xu, 2003. Remote sensing of forests over time, *Remote Sensing of Forest Environments: Concepts and Case Studies* (M.A. Wulder and S.E. Franklin, editors), Kluwer.
- Huang, C., B. Wylie, L. Yang, C. Homer, and G. Zylstra, 2000. Derivation of a Tasseled Cap Transformation Based on Landsat 7 At-Satellite Reflectance, Raytheon ITSS, USGS EROS Data Center, Sioux Falls, South Dakota, URL: <http://landcover.usgs.gov/pdf/tasseled.pdf> (last date accessed: 12 March 2008).
- Im, J., J. Rhee, J.R. Jensen, and M.E. Hodgson, 2007. An automated binary change detection model using a calibration approach, *Remote Sensing of Environment*, 106(1):89–105.
- Jensen, J.R., 2005. *Introductory Digital Image Processing: A Remote Sensing Perspective*, Third edition, Upper Saddle River, New Jersey, Pearson Prentice Hall.
- Jin, S., and S.A. Sader, 2005. MODIS time-series for forest disturbance detection and quantification of patch size effects, *Remote Sensing of Environment*, 99(4):462–470.



Legend

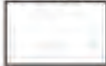




-  Polygon Layer
-  Manual GIS Change
-  MODIS Polygon-Based Change
-  MODIS Pixel-Based Change
-  Area of Interest

Plate 4. Examples of the limitations of pixel size and location. The green circle highlights one example of the effectiveness and the challenges of detecting well-sites using MODIS. The challenges are mainly associated with pixel location, pixel size, and polygon shape.

Justice, C.O., J.R.G. Townshend, E.F. Vermote, E. Masuoka, R.E. Wolfe, N. Saleous, D.P. Roy and J.T. Morisette, 2002. An overview of MODIS Land data processing and product status, *Remote Sensing of Environment*, 83(1–2):3–15.

Kasischke, E.S., and N.H. French, 1995. Locating and estimating the aerial extent of wildfires in Alaskan boreal forests using multiple-season AVHRR NDVI composite data, *Remote Sensing of Environment*, 51(2):263–275.

Le Hégarat-Mascel, S., C. Otle, and C. Guerin, 2005. Land cover change detection at coarse spatial scales based on iterative estimation and previous state information, *Remote Sensing of Environment*, 95(4):464–479.

Lunetta, R.S., D.M. Johnson, J.G. Lyon, and J. Crowell, 2004. Impacts of imagery temporal frequency on land-cover change detection monitoring, *Remote Sensing of Environment*, 89(4):444–454.

- Lunetta, R.S., and C.D. Elvidge, 1998. *Remote Sensing Change Detection: Environmental Monitoring Methods and Applications*, Ann Arbor Press, Chelsea, Michigan.
- Lyon, J., D. Yuan, R. Lunetta, and C. Elvidge, 1998. A change detection experiment using vegetation indices, *Photogrammetric Engineering & Remote Sensing*, 64(1):143–150.
- Mas, J.F., 1999. Monitoring land cover changes: A comparison of change detection techniques, *International Journal of Remote Sensing*, 20(1):139–152.
- McDermid, G.J., S.E. Franklin, and E.F. LeDrew, 2005. Remote sensing for large-area habitat mapping, *Progress in Physical Geography*, 29(4):449–474.
- Moody, A., and D.M. Johnson, 2001. Land surface phonologies from AVHRR using the discrete Fourier transform, *Remote Sensing of Environment*, 75(3):305–323.
- Olsen, K., P. Collas, P. Boileau, D. Blain, C. Ha, L. Hendersen, C. Liang, S. McKibbin, and L. Morel-à-l'Huissier, 2002. *Canada's Greenhouse Gas Inventory (1990–2000)*, Greenhouse Gas Division, Environment Canada, URL: http://www.ec.gc.ca/pdb/ghg/inventory_report/1990_00_report/source/031_ghgas_english5.pdf (last date accessed: 12 March 2008).
- Stenhouse, G.B., and K. Graham, 2005. *Foothills Model Forest Grizzly Bear Research Program: 1999–2003 Final Report*, Unpublished.
- Tansey, K., J.M. Gregoire, E. Binaghi, L. Boschetti, P.A. Brivio, D. Ershov, S. Flasse, R. Fraser, D. Graetz, M. Maggi, P. Peduzzi, J. Pereira, J. Silva, A. Sousa, and D. Stroppiana, 2004. A global inventory of burned areas at 1 km resolution for the year 2000 derived from SPOT VEGETATION data, *Climatic Change*, 67(2–3):345–377.
- Thenkabail, P.S., M. Schull, and H. Turrall, 2005. Ganges and Indus river basin land-use/land cover (LULC) and irrigated area mapping using continuous streams of MODIS data, *Remote Sensing of Environment*, 95(3):317–341.
- Toutin, T., 1995. Multisource data integration: Comparison of geometric and radiometric methods, *International Journal of Remote Sensing*, 16(15):2795–2811.
- Townshend, J.R., and C.O. Justice, 2002. Towards operational monitoring of terrestrial systems by moderate-resolution remote sensing, *Remote Sensing of Environment*, 83(1–2): 351–359.
- Wessels, K.J., R.S. De Fries, J. Dempewolf, L.O. Anderson, A.J. Hansen, S.L. Powell, and E.F. Moran, 2004. Mapping regional land cover with MODIS data for biological conservation: Examples from the Greater Yellowstone ecosystem, USA and Pará State, Brazil, *Remote Sensing of Environment*, 92(1):67–83.
- Wulder, M.A., J.A. Dechka, M.A. Gillis, J.E. Luther, R.J. Hall, A. Beaudoin, and S.E. Franklin, 2003. Operational mapping of the land cover of the forested area of Canada with Landsat data: EOSD land cover program, *The Forestry Chronicle*, 79(6):1075–1083.
- Wulder, M.A., W.A. Kurz, and M. Gillis, 2004. National level forest monitoring and modeling in Canada, *Progress in Planning*, 61:365–381.
- Yuan, D., C.D. Elvidge, and R.S. Lunetta, 1998. Survey of multispectral methods for land cover change analysis, *Remote Sensing Change Detection, Environmental Monitoring Methods and Applications* (R.S. Lunetta and C.D. Elsevier, editors), Ann Arbor Press, Chelsea, Michigan.
- Zhan, X., R.A. Sohlberg, J.R.G. Townshend, C. DiMiceli, M.L. Carroll, J.C. Eastman, M.C. Hansen, and R.S. Defries 2002. Detection of land cover changes using MODIS 250 m data, *Remote Sensing of Environment*, 83(1–2):336–350.

(Received 22 September 2006; accepted 13 February 2007; revised 14 May 2007)